Germanium nanospheres for ultraresolution picotensiometry of kinesin motors

Swathi Sudhakar[1], Mohammad Kazem Abdosamadi[1], Tobias Jörg Jachowski[1], Michael Bugiel[1], Anita Jannasch[1] & Erik Schäffer[1,⋆]

[1]*Eberhard Karls Universität Tübingen, ZMBP, Auf der Morgenstelle 32, 72076 Tübingen, Germany*

⋆*Corresponding author: erik.schaeffer@uni-tuebingen.de*

Force spectroscopy on single molecular machines generating piconewton forces is often performed using optical tweezers.[1–3] Since optical forces scale with the trapped particle volume, piconewton force measurements require micron-sized probes practically limiting the spatiotemporal resolution.[1,2,4,5] Here, we have overcome this limit by developing high-refractive index germanium nanospheres as ultraresolution trapping probes. Using these probes, we have dissected the molecular motion of the cytoskeletal motor kinesin-1 that transports vesicles along microtubule filaments. With a superior spatiotemporal resolution, we have resolved a controversy unifying its stepping and detachment behavior. We found that single motors took 4-nm-center-of-mass steps with alternating force dependence of their dwell times. At maximum force, motors did not detach but switched to a weakly bound state. In this state, mo-

tors slid on the microtubule with 8-nm steps on a microsecond time scale. Kinesins remained in this intermediate slip state before either truly detaching or reengaging in directed motion. Surprisingly, reengagement and, thus, rescue of directed motion occurred in about 80 percent of events. Such rescue events suggest that macroscopically observed run lengths of individual motors are concatenations and rescues need to be accounted for to understand long-range transport. Furthermore, teams of motors involved in transport may be synchronized through the weakly bound slip state. Apart from ultraresolution optical trapping, germanium nanospheres are promising candidates for applications ranging from nanophotonics to energy storage.

Molecular motors and trapping probes are subjected to Brownian motion that fundamentally limits the spatiotemporal resolution of optical tweezers.[5] By temporal averaging over this motion, discrete motor steps of size δ and the time between steps—the dwell time τ—can be resolved. Such single-molecule measurements have provided unprecedented insight into essential mechanochemical processes of life.[1–3] However, many such processes cannot be measured at their native spatiotemporal resolution but only under conditions—for example, low nucleotide concentrations—at which the mechanochemistry is slowed down and might be different.[6] For example, the benchmark, 3.4-Å–DNA-base-pair-sized steps of the RNA polymerase, naturally operating on a millisecond time scale, could only be resolved on a second time scale.[7] The inherent trade-off between temporal and spatial

precision and the resolution limit itself are quantified by the product $\delta\sqrt{\tau}$ that has a constant value, with the lower limit hardly depending on the experiment.[2,5] Thus, this relation implies that detecting 8-nm steps of a kinesin motor on a millisecond time scale is as challenging as measuring Å-steps on a second time scale. Furthermore, apart from reducing linker compliance between probe and molecular machine, spatiotemporal resolution can only be significantly improved relative to the benchmark by the use of nanometer-sized optical trapping probes.[2,5] However, such probes for piconewton-force measurements do not exist.

Cytoskeletal motors like kinesins drive many essential cellular processes by coupling ATP hydrolysis to perform mechanical work.[8] During an ATP hydrolysis cycle, kinesin motors advance by 8 nm along microtubules against forces of several piconewtons via a rotational hand-over-hand mechanism.[6,9] While consensus develops on how kinesin motors work[10,11] important details remain unclear. For example, it is controversial whether intermediate mechanical steps in the hydrolysis cycle exist and can support load.[12–17] Furthermore, to enhance transport in crowded cells, kinesin motors work cooperatively in small teams.[18–20] Key for team performance is how loads due to unsynchronized or opposing motors and obstacles affect transport distance.[18–21] This distance and force generation are limited by motor detachment. However, how kinesins detach from microtubules is not known.[19,21]

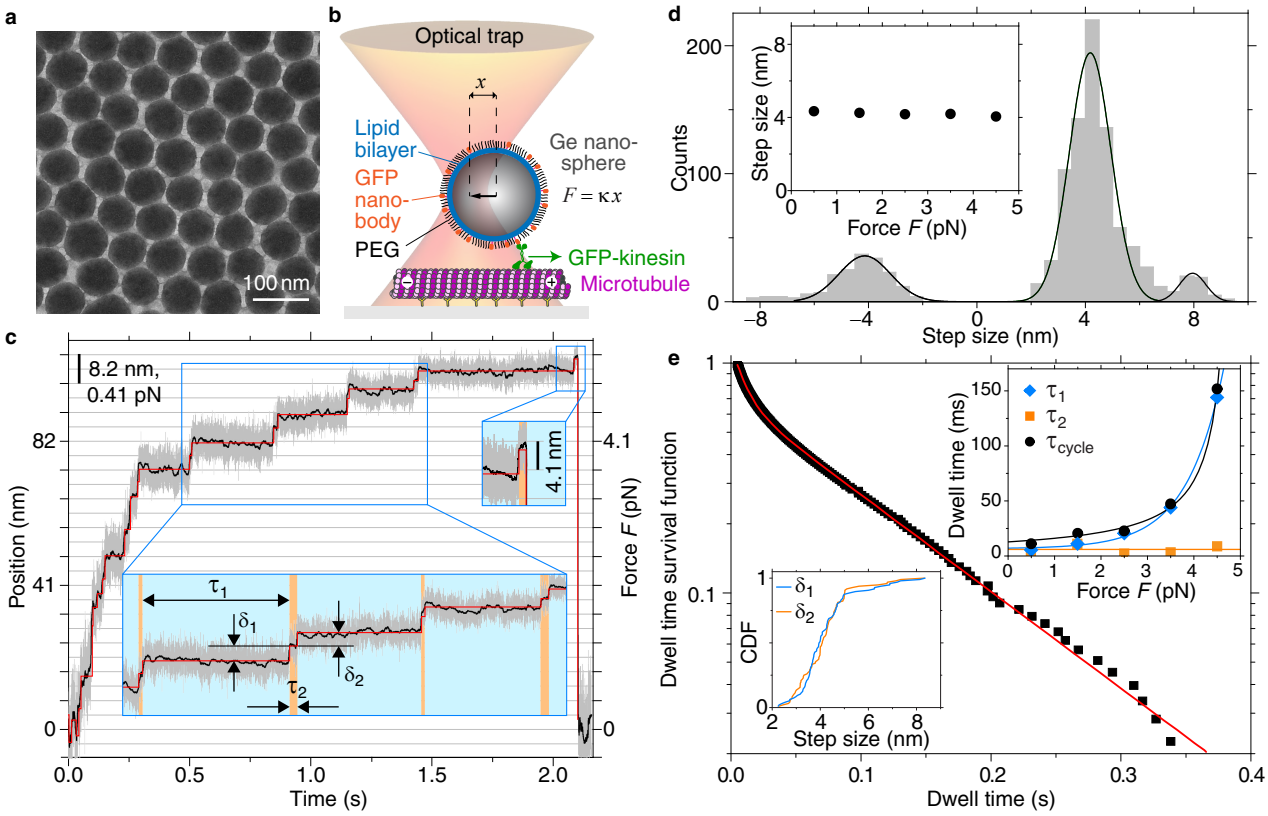

Fig. 1 | Ultraresolution kinesin traces employing optically trapped germanium nanospheres. **a**, TEM image of ≈70 nm germanium nanospheres (GeNTOPs). **b**, Schematic of a kinesin motor transporting a functionalized GeNTOP along a microtubule roughly drawn to scale including a section of a grey-shaded 0.59 µm diameter microsphere for comparison (the optical trap is too small; see text and methods for details). **c**, Time trace for a single-kinesin powered GeNTOP (100 kHz bandwidth, grey trace; filtered data, ≈100 Hz, black trace; detected steps, red line; see methods). Insets: magnified view of last and intermediate steps with definition of long and short dwell times τ_1 (blue shaded) and τ_2 (orange shaded) with corresponding step sizes δ_1 and δ_2, respectively. **d**, Step size histogram with a multi-Gaussian fit (line). Inset: Dominant step size versus force. **e**, Dwell time distribution of steps for *F* between 2–3 pN with fit (red line). Inset: Dwell times (symbols) with models (lines) versus force (top right, see methods); and cumulative distribution function (CDF) of alternating step sizes (bottom left).

Germanium nanospheres for ultraprecision spatiotemporal measurements

To resolve how kinesin steps and detaches, we enhanced the spatiotemporal precision of optical tweezers by compensating the particle-volume-scaling of trapping forces in the Rayleigh regime with the use of highest infrared refractive index **ge**rmanium **n**anospheres as **t**rappable **o**ptical **p**robes (GeNTOPs). While various methods exist to make semiconductor nanoparticles,[22–26] none provide water-stable, monodisperse, sufficiently large nanospheres for picotensiometry in adequate amounts. The synthesis that we developed derives from a solution-based method[24] and resulted in uniform GeNTOPs with a size of 72.0 ± 0.8 nm (mean $\pm$ standard error unless noted otherwise, $N = 100$) measured by transmission electron microscopy (TEM, Fig. 1a, see methods for details). To determine whether the spatiotemporal trapping precision of GeNTOPs was improved compared to commonly used microspheres, we trapped GeNTOPs in an ultrastable optical tweezers setup[27] (Extended Data Fig. 1) and calibrated them by a combined power spectral density–drag force method[28,29] (Extended Data Fig. 2). The GeNTOP calibration showed that we achieved the optical-trap spring constant—the trap stiffness κ—necessary for kinesin picotensiometry employing microspheres.[6,9,12–14] Also, for the used laser power, the trap stiffness quantitatively agreed with a Mie theory calculation based on the dielectric properties of germanium at the infrared trapping laser wavelength (see methods). Thus, GeNTOPs had indeed the expected very high refractive index of 4.34. In summary, be-

cause of the GeNTOPs' high refractive index and nanometric size, spatial precision is significantly improved and the trap response time reduced by about an order of magnitude to $\tau_{\text{trap}} = (2\pi f_c)^{-1} = \gamma/\kappa \approx 10\,\mu\text{s}$, where f_c is the corner frequency and γ is the drag coefficient (Extended Data Fig. 2). By using a higher trap stiffness and/or smaller GeNTOPs, the response time can be reduced further.

Membrane-coated GeNTOPs for kinesin transport

To mimic *in vivo* vesicles while minimizing linker compliance and nonspecific interactions, we coated GeNTOPs with a PEGylated lipid bilayer functionalized with nanobodies that bound truncated, recombinant green-fluorescent-protein-(GFP)-tagged kinesin-1 motors hereafter called kinesin (Fig. 1b, Extended Data Fig. 3, see methods). The functionalization increased the GeNTOP diameter to $93 \pm 4\,\text{nm}$ according to dynamic light scattering. This diameter corresponds to the average size of neuronal transport vesicles.[18] Thus, dimensions and the force geometry when using GeNTOPs resemble conditions inside cells. By using a low motor-to-GeNTOP ratio for further optical tweezers experiments, we ensured that only single kinesins transported GeNTOPs along microtubules with the expected speed and run length quantified by interference reflection microscopy[30] (Extended Data Fig. 3, see methods).

Kinesin takes 4-nm steps

To dissect the kinesin gait, we trapped single-kinesin-functionalized GeNTOPs at physiological ATP concentrations, placed them on microtubules, and recorded the kinesin-powered GeNTOP displacement from the trap centre (Fig. 1b). Based on this displacement x within the linear response of the GeNTOPs (inset Extended Data Fig. 2), the Hookean spring load of the optical tweezers corresponds to a force $F = \kappa x$. In the exemplary trace of Fig. 1c (see more examples in Extended Data Fig. 4), motors slowed down with increasing force up to ≈5 pN. Also with increasing force, stepwise motion became more evident until GeNTOPs quickly returned to the trap centre (in Fig. 1c at ≈2.1 s). To determine step sizes and dwell times, we used an efficient, automated filtering and step finding algorithm (see methods). Remarkably, instead of 8-nm steps,[9] most forward-directed, centre-of-mass steps were 4.12 ± 0.03 nm (centre of Gaussian ± fit error) consistent with the size of a tubulin monomer. Because step size hardly depended on force (inset Fig. 1d, Extended Data Fig. 5), the combined linker-motor compliance was very low such that we could pool all steps together (Fig. 1d). There were only a few 8-nm forward and some 4-nm, but hardly any 8-nm, backward steps (Extended Data Table 1). Thus, our data directly shows that kinesin walks with 4-nm centre-of-mass steps and that intermediate steps can support load. Interestingly, for increasing forces, the step duration appeared to be alternating between a long and short dwell time that we denote by τ_1 and τ_2, respectively (Fig. 1c).

Quantitatively, dwell time survival functions pooled from different force intervals were consistent with either a single exponential or sum of two exponentials with approximately equal amplitude for forces below or above 2 pN, respectively (Fig. 1e, Extended Data Table 1). Equal amplitudes imply that both type of dwells occurred equally often consistent with alternating steps having different properties. While the first dwell time τ_1 depended on force, the second one, τ_2, hardly depended on force (blue and orange lines in top right inset Fig. 1e, see methods). The sum of the two dwell times τ_{cycle} was consistent with a model based on the force-dependent speed of the motor (black circles and line in top right inset Fig. 1e, see methods) suggesting that each hydrolysis cycle is broken up into two mechanical substeps. Data recorded at low ATP concentrations (Fig. 2, see methods), show that only the first dwell time τ_1 that depended on force also depended on ATP while τ_2-values at low ATP hardly differed from the high-ATP values (Extended Data Table 1 and 2). Furthermore, for forces larger than 3 pN and physiological ATP concentrations, for which we could clearly assign alternating steps, the step size of alternating steps, always measured after the dwell, did not differ significantly (δ_1 = 4.03 $\pm$ 0.06 nm, N = 97 and δ_2 = 3.94 $\pm$ 0.06 nm, N = 88 for τ_1 and τ_2, respectively, bottom left inset Fig. 1e). However, we cannot rule out that the distributions consist of two closely spaced Gaussians with means that differ by the offset distance between neighboring protofilaments. Nevertheless, kinesin motors walked on average with 4-nm center-of-mass steps alternating in the force

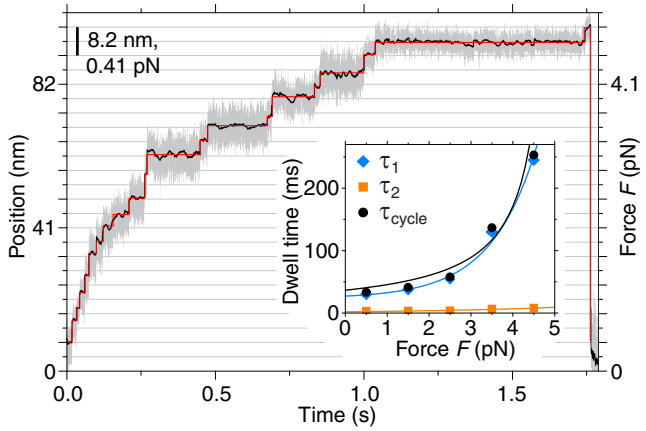

Fig. 2 | Low-ATP-concentration kinesin trace. Time trace for a single-kinesin powered GeNTOP at 10 µM ATP (100 kHz bandwidth, grey trace; filtered data, ≈100 Hz, black trace; detected steps, red line; see methods). Inset: Dwell times (symbols) with models (lines) versus force (see methods).

and ATP dependence of their dwell times.

Kinesin detachment and motility rescue

How and from which substep do motors detach? We noticed that in about 50 % of the motility events (N = 149), the last step—before the GeNTOP quickly returned to the trap centre—was a short substep (Fig. 1c, Extended Data Fig. 4). For the subsequent fast backward motion, we expected an exponential relaxation with a time constant corresponding to the trap response time τ_{trap} in case of microtubule-motor detachment.[8] However, while the backward motion directed along the microtubule axis could be fitted by an exponential relaxation (red line in Fig. 3a), the average time constant $\tau_{\parallel}$ = 295 ± 9 µs (N = 149)—

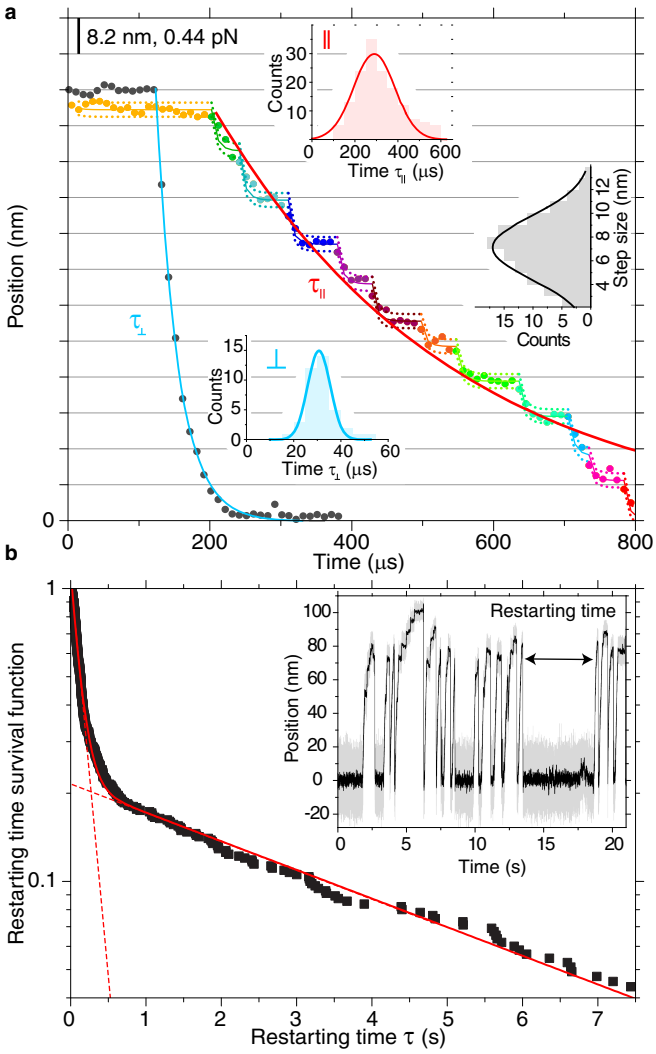

Fig. 3 | Ultrafast steps and motility rescue. a, Magnified time traces for a single-kinesin powered GeNTOP after the last step (grey and multicolored circles with or without sideward load, respectively, 100 kHz bandwidth) with single exponential fits (blue and red line for motion perpendicular ($\perp$) and parallel ($\parallel$) to the microtubule axis, respectively). Multicolored lines correspond to states detected by a change-point algorithm[31] (dotted line 95 % confidence interval). Inset: histograms with Gaussian fits (solid lines) of relaxation time constants $\tau_{\parallel}$ and $\tau_{\perp}$ (same color code as single exponential fits) and step size for detected states. **b**, Restarting-time distribution (squares) fitted with a sum of two exponentials (line with dashed line extrapolation, N = 550). Inset: Illustration of the restarting time between consecutive kinesin motility events.

and all individual ones without exception—was much larger than the trap response time. This discrepancy suggests that the kinesin still interacted with the microtubule (Fig. 3a). To prevent microtubule interactions after the last step, we additionally pulled sideways on the kinesin-coated GeNTOP during motility events. With a load perpendicular to the microtubule axis, the relaxation time $\tau_\perp$ after the last step was only 30.7 $\pm$ 0.8 µs (N = 50) consistent with the expected trap relaxation time in the proximity of the surface[29] and true motor detachment (Extended Data Fig. 6). Close inspection of the relaxation traces along the microtubule (without sideward loads) revealed steps occurring on a microsecond time scale that were robustly detected by an unbiased change-point detection algorithm[31] (Fig. 3a and further examples in Extended Data Fig. 7 and 8, see methods). Individual steps were composed of an exponential relaxation with a time constant of 27 $\pm$ 3 µs (N = 20) consistent with the trap relaxation time τ_{trap} and had a step size of 7.2 $\pm$ 0.2 nm (N = 111) close to the 8 nm repeat of the microtubule lattice (inset Fig. 3a) with a dwell time of 71 $\pm$ 4 µs (N = 124) averaged over all forces. Thus, we conclude that during fast backward motion, motors switched to a weakly bound slip state and remained in contact with the microtubule lattice. To determine whether motors truly detached from this weakly bound state or whether motors could switch back to a motility-competent state, we analyzed the time between subsequent motility events that we call restarting time (inset Fig. 3b). Intriguingly, also the restarting time survival function was well described by a sum of two

exponentials having a time constant of 112 ± 1 ms and 4.1 ± 0.4 s, respectively (Fig. 3b). Two time constants imply that motility events started from two different states, possibly being *de novo* binding and the weakly bound state. The short restarting time constant that we measured is in excellent agreement with the one of a predicted weakly bound state prior to detachment of duration 131 ± 14 ms.[21] Surprisingly, 82 ± 1 % of our events had this short restarting time constant suggesting that most motors did not detach but motility was rescued from the weakly bound state.

Our data is consistent with a model for kinesin stepping that splits up the hydrolysis cycle into two mechanical substeps. In between the substeps, the motor can branch off from the normal hydrolysis pathway and switch to a weakly bound diffusive or sliding state prior to detachment or rescue of motility (Fig. 4). Overall, our model builds on and expands previous models.[6,10,11,16,32] Initially, both motor heads are bound to the microtubule with ADP and inorganic phosphate (P_i) in the rear head and no nucleotide in the front one. With P_i release from the rear head and ATP binding to the other one, the rear neck linker is un- and the front one docked. This process triggers the first 4-nm, ATP-dependent centre-of-mass substep (Substep $\tau_1(F,\mathrm{ATP})$ in Fig. 4). Since load is acting on the front neck linker during docking, it may explain that the dwell time of this step is also force dependent. Upon ATP hydrolysis in the front and ADP release from the rear head, the hydrolysis cycle is completed with a second 4-nm substep (Substep τ_2 in Fig. 4). Since

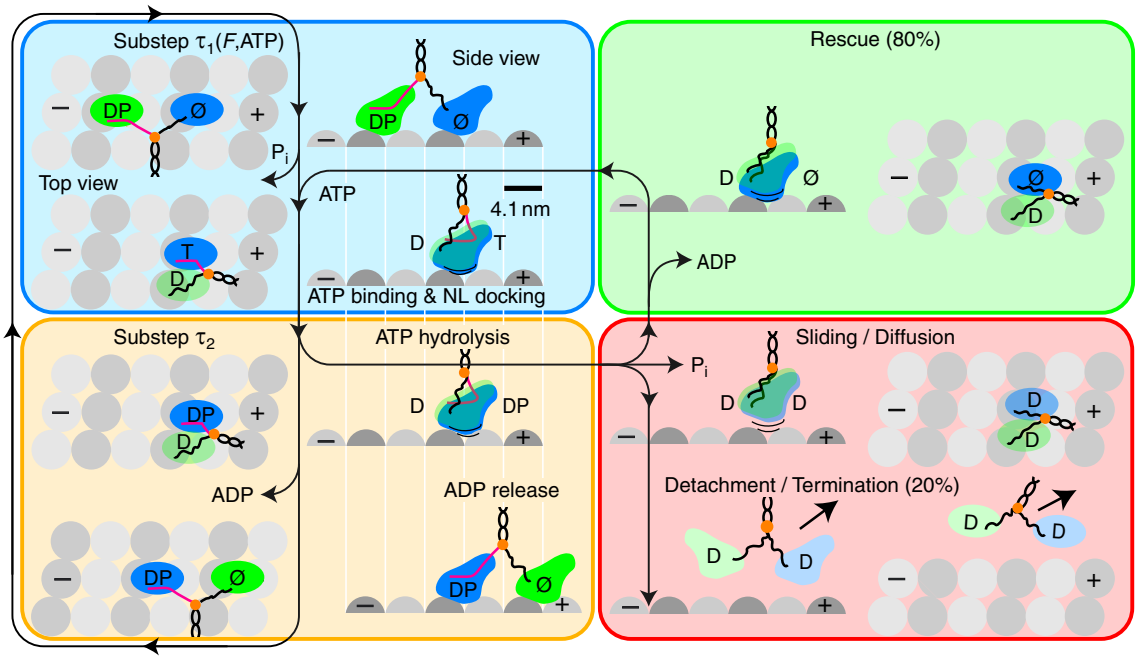

Fig. 4 | Hydrolysis cycle with detachment and rescue. Top and side view of kinesin with two identical heads (blue and green) stepping along a microtubule (grey spheres mark tubulin monomers). The hydrolysis cycle is divided into a force-dependent (blue box) and hardly force-dependent (orange box) substep with dwell times $\tau_1(F,\mathrm{ATP})$ and τ_2, respectively. Between these substeps, motors may switch to a weakly bound sliding or diffusive state from which motors either detach (red box) or motility is rescued (green box). The centre of mass is indicated by an orange circle, a docked neck linker (NL) marked by a magenta line, weak binding by lines underneath the heads, and nucleotide states by T: ATP, D: ADP, P: inorganic phosphate, and Ø: nucleotide free.

.

ATP is already bound, this substep does not depend on the ATP concentration. Also, because load is mainly acting on the rear head through the docked neck linker and the front head is free to perform a diffusive search with an undocked neck linker, may explain why the dwell time of this step is hardly force dependent (inset Fig. 1e and Fig. 2). Based on previous[6] and our current data, we suggest that heads always remain weakly bound to the microtubule lattice likely due to electrostatic interactions, for example, with the negatively charge E-hooks of tubulin. If P_i is released from the front head directly after ATP hydrolysis and before ADP is released from the rear head, both heads enter a weakly bound, diffusive ADP state interrupting the normal hydrolysis cycle (red box in Fig. 4). Load will bias such a diffusive state, as observed for the fast backward sliding motion after the last kinesin step when stalling, resulting in stepwise sliding motion opposed by hydrodynamic drag and protein friction.[33] The measured step size of these fast, sliding steps close to 8 nm suggests that the motor heads interact primarily with the canonic kinesin-microtubule binding site. While we hardly observe 8-nm backward steps, we observed some short slip events (Extended Data Fig. 8). With a different force geometry and large microspheres that cause a large drag, such events may correspond to previously observed backward steps.[14] Protein friction allows us to estimate the diffusive step dwell time during the fast sliding motion. Based on the time constant for the fast movement back to the trap centre $\tau_{\parallel} = \tau_{\text{trap}} + \gamma_{\text{protein friction}}/\kappa$, the force-averaged friction coefficient due to friction between

the motor and its track is $\gamma_{\text{protein friction}} \approx 15\,\text{nN s/m}$ and the corresponding diffusion coefficient according to the Einstein relation is $D = k_\text{B}T/\gamma_{\text{protein friction}} \approx 0.3\,\mu\text{m}^2/\text{s}$, where k_B is the Boltzmann constant and T the absolute temperature. Furthermore, if we model the backward movement by a biased one-dimensional random walk with a step size of δ = 8 nm, the expected average step time is $\tau \approx \delta^2/(2D) \approx 70\,\mu\text{s}$. This time constant is in excellent agreement with the directly measured dwell time during the fast backward sliding motion (Fig. 3a) and supports the notion of a biased weakly bound slip state prior to detachment or rescue.[21] Unexpectedly, in only roughly 20 % of events, motors did truly detach, but in 80 % of the cases ADP must have dissociated from one of the heads rescuing directed motion. We expect that motors also switch to this diffusive state when no load is applied, suggesting that overall run lengths of motors are concatenations of processive runs interrupted by short diffusive periods.[34,35]

Relative to the benchmark,[7] the spatiotemporal resolution $\delta\sqrt{\tau}$ of the fast 8-nm steps on microsecond time scales, is an improvement by a factor of about 4.5× and 20× with respect to spatial and temporal resolution (Extended Data Fig. 9). Thus, GeNTOPs do allow to observe molecular machines at their native spatiotemporal resolution. In our case, the dwell time of the weakly bound state cannot be slowed down by reducing nucleotide concentrations because nucleotides likely did not exchange during sliding. For kinesins, the detachment and rescue state allows motors to slide back to their team during transport

with direct reengagement in motility. This process provides a route for load distribution and motor synchronization enhancing transport. Therefore, for a better understanding of long-range transport in crowded cells[19] and, in general, other essential cellular functions of kinesins, the sliding and rescue processes need to be accounted for. GeNTOPs not only break limits in optical trapping, but open up many other opportunities due to having the highest infrared refractive index of common materials and being a semiconductor. Germanium nanospheres are a lower-toxicity alternative to compound semiconductor nanoparticles,[22,24] optimal for bioimaging and sensing at wavelengths biological tissues are transparent,[23] promising candidates for other applications in nanophotonics and optoelectronics,[25,26] and may enhance energy harvesting and storage.[36] Widely available, size-controllable high-refractive index nanospheres will pave the way for many new discoveries and technologies.

1. Svoboda, K. & Block, S. M. Biological applications of optical forces. *Annu. Rev. Biophys. Biomol. Struct.* **23**, 247–285 (1994).

2. Moffitt, J. R., Chemla, Y. R., Smith, S. B. & Bustamante, C. Recent advances in optical tweezers. *Annu. Rev. Biochem.* **77**, 205–228 (2008).

3. Gennerich, A. *Optical Tweezers*. Methods Mol. Biol. (Springer, New York, 2017).

4. Ashkin, A., Dziedzic, J. M., Bjorkholm, J. E. & Chu, S. Observation of a single-beam gradient force optical trap for dielectric particles. *Opt. Lett.* **11**, 288–290 (1986).

5. Gittes, F. & Schmidt, C. F. Signals and noise in micromechanical measurements. In Sheetz, M. P. (ed.) *Methods Cell Biol.*, vol. 55, 129–156 (Academic Press, 1997).

6. Ramaiya, A., Roy, B., Bugiel, M. & Schäffer, E. Kinesin rotates unidirectionally and generates torque while walking on microtubules. *Proc. Natl. Acad. Sci. USA* **114**, 10894–10899 (2017).

7. Abbondanzieri, E. A., Greenleaf, W. J., Shaevitz, J. W., Landick, R. & Block, S. M. Direct observation of base-pair stepping by RNA polymerase. *Nature* **438**, 460–465 (2005).

8. Howard, J. *Mechanics of motor proteins and the cytoskeleton* (Sinauer Associates, Sunderland, MA, 2001).

9. Svoboda, K., Schmidt, C. F., Schnapp, B. J. & Block, S. M. Direct observation of kinesin stepping by optical trapping interferometry. *Nature* **365**, 721–727 (1993).

10. Hancock, W. O. The Kinesin-1 Chemomechanical Cycle: Stepping Toward a Consensus. *Biophys. J.* **110**, 1216–1225 (2016).

11. Cross, R. A. Review: Mechanochemistry of the kinesin-1 ATPase. *Biopolymers* **105**, 476–482 (2016).

12. Coppin, C. M., Finer, J. T., Spudich, J. A. & Vale, R. D. Detection of sub-8-nm movements of kinesin by high-resolution optical-trap microscopy. *Proc. Natl. Acad. Sci. U. S. A.* **93**, 1913–1917 (1996).

13. Nishiyama, M., Muto, E., Inoue, Y., Yanagida, T. & Higuchi, H. Substeps within the 8-nm step of the ATPase cycle of single kinesin molecules. *Nat. Cell Biol.* **3**, 425–428 (2001).

14. Carter, N. J. & Cross, R. A. Mechanics of the kinesin step. *Nature* **435**, 308–312 (2005).

15. Block, S. M. Kinesin motor mechanics: Binding, stepping, tracking, gating, and limping. *Biophys. J.* **92**, 2986–2995 (2007).

16. Mickolajczyk, K. J. *et al.* Kinetics of nucleotide-dependent structural transitions in the kinesin-1 hydrolysis cycle. *Proc. Natl. Acad. Sci. USA* **112**, E7186–E7193 (2015).

17. Isojima, H., Iino, R., Niitani, Y., Noji, H. & Tomishige, M. Direct observation of intermediate states during the stepping motion of kinesin-1. *Nat. Chem. Biol.* **12**, 290–297 (2016).

18. Hendricks, A. G. *et al.* Motor coordination via a tug-of-war mechanism drives bidirectional vesicle transport. *Curr. Biol.* **20**, 697–702 (2010).

19. Feng, Q., Mickolajczyk, K. J., Chen, G.-y. & Hancock, W. O. Motor reattachment kinetics play a dominant role in multimotor-driven cargo transport. *Biophys. J.* **114**, 400–409 (2018).

20. Schimert, K. I., Budaitis, B. G., Reinemann, D. N., Lang, M. J. & Verhey, K. J. Intracellular cargo transport by single-headed kinesin motors. *Proc. Natl. Acad. Sci. USA* **116**, 6152–6161 (2019).

21. Khataee, H. & Howard, J. Force generated by two kinesin motors depends on the load direction and intermolecular coupling. *Phys. Rev. Lett.* **122**, 188101 (2019).

22. Fan, J. & Chu, P. K. Group IV nanoparticles: Synthesis, properties, and biological applications. *Small* **6**, 2080–2098 (2010).

23. Vaughn II, D. D. & Schaak, R. E. Synthesis, properties and applications of colloidal germanium and germanium-based nanomaterials. *Chem. Soc. Rev.* **42**, 2861–2879 (2013).

24. Guo, Y. J. *et al.* Facile synthesis of multifunctional germanium nanoparticles as a carrier of quercetin to achieve enhanced biological activity. *Chem. Asian J.* **9**, 2272–2280 (2014).

25. Kuznetsov, A. I., Miroshnichenko, A. E., Brongersma, M. L., Kivshar, Y. S. & Luk'yanchuk, B. Optically resonant dielectric nanostructures. *Science* **354**, aag2472 (2016).

26. Krasnok, A., Caldarola, M., Bonod, N. & Alú, A. Spectroscopy and biosensing with optically resonant dielectric nanostructures. *Adv. Opt. Mater.* **6**, 1701094 (2018).

27. Mahamdeh, M. & Schäffer, E. Optical tweezers with millikelvin precision of temperature-controlled objectives and base-pair resolution. *Opt. Express* **17**, 17190 (2009).

28. Tolic-Nørrelykke, S. F., Schäffer, E., Howard, J., Pavone, F. S. & Jülicher, F. Calibration of optical tweezers with positional detection in the back focal plane. *Rev. Sci. Instrum.* **77**, 103101 (2006).

29. Schäffer, E., Nørrelykke, S. F. & Howard, J. Surface forces and drag coefficients of microspheres near a plane surface measured with optical tweezers. *Langmuir* **23**, 3654–3665 (2007).

30. Simmert, S., Abdosamadi, M., Hermsdorf, G. & Schäffer, E. LED-based interference-reflection microscopy combined with optical tweezers for quantitative three-dimensional microtubule imaging. *Opt. Express* **26**, 1437–1448 (2018).

31. Wiggins, P. A. An information-based approach to change-point analysis with applications to biophysics and cell biology. *Biophys. J.* **109**, 346–354 (2015).

32. Andreasson, J. O. L. *et al.* Examining kinesin processivity within a general gating framework. *eLife* **21**, 1–22 (2015).

33. Bormuth, V., Varga, V., Howard, J. & Schäffer, E. Protein friction limits diffusive and directed movements of kinesin motors on microtubules. *Science* **325**, 870–874 (2009).

34. Jannasch, A., Bormuth, V., Storch, M., Howard, J. & Schäffer, E. Kinesin-8 is a low-force motor protein with a weakly bound slip state. *Biophys. J.* **104**, 2456–2464 (2013).

35. Chugh, M. *et al.* Phragmoplast orienting kinesin 2 is a weak motor switching between processive and diffusive modes. *Biophys. J.* **115**, 375–385 (2018).

36. Kim, T. H., Song, H. K. & Kim, S. Production of germanium nanoparticles via laser pyrolysis for anode materials of lithium-ion batteries and sodium-ion batteries. *Nanotechnology* **30**, 275603 (2019).

37. Jannasch, A., Mahamdeh, M. & Schäffer, E. Inertial effects of a small brownian particle cause a colored power spectral density of thermal noise. *Phys. Rev. Lett.* **107**, 228301 (2011).

Methods

Synthesis of germanium nanospheres (GeNTOPs) The germanium nanospheres were synthesized in an aqueous solution advancing a method of Guo *et al.*[24] As substrate, 17.0 mg of germanium oxide (GeO_2) and 96.0 mg of quercetin, acting as a stabilizing agent, were dissolved in 10 ml of a 0.15 M sodium hydroxide solution each and then mixed together while stirring for 10 min and adjusting the pH to 8.8 via titration with 37 % HCl (Solution A). Subsequently, 29.5 mg of sodium borohydride ($NaBH_4$, reducing agent) was dissolved as quickly as possible in 3 ml of 4 °C-cold water and stored in a refrigerator at 4 °C (Solution B). Then, Solution A was stirred continuously in a preheated oil bath at 60 °C for 10 min and Solution B was added dropwise. The reaction was stopped after 5 h and GeNTOPs washed thrice thoroughly with water by centrifuging the sample at 13,000 rpm. All chemicals were purchased from Sigma Aldrich and used without further purification unless noted otherwise. Purified Type 1 water was used for all experiments (18.2 MΩ cm, Nanopure System MilliQ reference with Q-POD and Biopak filter). The size characterization analysis was done using a TEM-Jeol 1400 plus transmission electron microscope. About 10 µl of the GeNTOP solution was sonicated and subsequently 5 µl spotted on a TEM grid. Dynamic light scattering resulted in a diameter of 74 ± 3 nm consistent with the value obtained by TEM.

Lipid-bilayer functionalization of GeNTOPs After the synthesis, GeNTOPs were coated with a lipid bilayer using established methods.[38–40] Briefly, 1,2-dimyristoyl-sn-glycero-3-phosphocholine (DMPC, Avanti Polar Lipids, Inc.) and 1,2-distearoyl-sn-glycero-3-phosphoethanolamine-N-[carboxy(polyethylene glycol)-2000] (DSPE-COOH, Avanti Polar Lipids, Inc.) were dissolved in chloroform (10 mg/ml). Aliquots of a 4:1 molar ratio mixture of these lipids were dried overnight in a desiccator at 50 mbar and stored at −20 °C. The dried lipid mixture was hydrated by adding 1 ml of 80 °C warm buffer (10 mM 4-(2-hydroxyethyl)-1-piperazineethanesulfonic acid (HEPES), 150 mM NaCl, pH 7.4) resulting in a final total lipid concentration of about 0.5 mM. To form multilamellar vesicles (MLVs), the solution was mixed thoroughly by pipetting and vortexed for 2 min. Subsequently, small unilamellar vesicles (SUVs) were formed by sonicating the MLV mixture for 30 min at 80 °C. The sonicated solution was centrifuged at 12,000 rpm for 15 min and SUVs collected from the supernatant. Then, equal volumes of GeNTOP and SUV solutions were mixed. To induce fusion of the liposomes onto the GeNTOPs, $CaCl_2$ was added to the mixture (3 mM final concentration) that was incubated for 45 min at 80 °C in a thermomixer using a shaking speed of 600 rpm. The membrane-coated GeNTOPs were washed thrice in three different buffers, first with Buffer 1 (25 mM HEPES, 200 mM NaCl, 1 mM tris(2-carboxyethyl)phosphine (TCEP), pH 7.4, 5 mM EDTA) followed by washing them in Buffer 2 (25 mM HEPES, pH 7.4, 100 mM NaCl, 0.25 mM $CaCl_2$) and then in

Buffer 3 (25 mM HEPES, pH 7.4, 25 mM NaCl, 1 mM TCEP, 0.25 mM $CaCl_2$). After each wash, GeNTOPs were collected by spinning the sample at 13,000 rpm for 15 min and gently resuspending them. After the last resuspension step, GeNTOPs were lyophilized and kept at 4 °C for later use. For membrane visualization, 10 µl of 2 µM DiI lipophilic dye was added when hydrating the lipid mixture used to coat GeNTOPs. As a control, 100 µl of uncoated GeNTOPs, was mixed with 10 µl of 2 µM DiI lipophilic dye and incubated for 45 min. After incubation, these GeNTOPs were washed thrice with water and suspended in 100 µl water. Both the coated GeNTOPs with the membrane dye and control GeNTOPs were imaged by a Leica TCS SP8 confocal microscope with an excitation wavelength of 565 nm. No fluorescence was observed for the control.

GeNTOP PEGylation and nanobody coupling For kinesin experiments, we PEGylated GeNTOPs and covalently bound GFP nanobodies to them as described previously[41] with some modifications. About 0.1 g of lyophylized GeNTOPs were dissolved in 1 ml water. From this stock, 25 µl were washed twice with 975 µl of 2-(N-morpholino)ethanesulfonic acid (MES) buffer (50 mM, pH = 6.0) by centrifuging GeNTOPs at 13,000 rpm for 15 min. Before each wash cycle, GeNTOPs were vortexed and sonicated in a bath sonicator for 15 s. Then, GeNTOPs were resuspended in 250 µl MES buffer. After washing, GeNTOPs were vortexed and sonicated for 180 s. Then, 16.4 mg of 1-(3-(dimethylamino)propyl)-3-ethylcarbodiimide hydrochloride (EDC) and 8.3 mg of N-hydroxysulfosuccinimide sodium

(NHS) were dissolved in 100 µl of MES buffer. From the prepared solution, 9 µl of NHS and 15.8 µl of EDC were added to the resuspended GeNTOPs and the solution was mixed in a thermomixer for 15 min at 37 °C. Then, GeNTOPs were washed twice with 500 µl of MES buffer, resuspended in 240 µl of PBS-T (phosphate buffer saline supplemented with 0.1 % Tween 20), and vortexed and sonicated for 90 s. Subsequently, GFP-nanobodies[42] (13 kDa, gift of Ulrich Rothbauer, NMI, Reutlingen, Germany) and 2 kDa α-methoxy-ω-amino PEG (Rapp Polymere, Tübingen, Germany) in a molar ratio of 1:1000 were coupled covalently to the GeNTOPs by incubating them in a thermomixer for 1 h at 600 rpm and 37 °C. Afterwards, GeNTOPs were washed five times with PBS-T and stored at 4 °C.

Sample preparation and assay Experiments were performed in flow cells that were constructed using silanized, hydrophobic glass cover slips and parafilm as described before[29,33] but chlorotrimethylsilane (Merck Millipore, Burlington, MA) was used to render surfaces hydrophobic. Truncated kinesin1-eGFP-6xHis (rk430) was purified as described previously.[6,33] Taxol-stabilized microtubules, sometimes additionally 10% rhodamine-labeled, were prepared as described previously.[43] Flow channels were washed with PEM buffer (80 mM 1,4-piperazinediethanesulfonic acid (PIPES), 1 mM EGTA, 1 mM $MgCl_2$, adjusted with KOH to pH 6.9), filled and incubated successively with anti β-tubulin I (monoclonal antibody SAP.4G5 from Sigma in PEM) for 15–20 min, Pluronic F-127 (1 % in PEM) for 20 min, and microtubules in PEM for 15 min. Kinesin with a stock concen-

tration of 12.1 mg/ml was diluted 1000× in motility buffer (PEM with 0.16 mg/ml casein, 1 mM or 10 µM ATP and an anti-fade cocktail [20 mM D-glucose, 0.02 mg/ml glucose oxidase, 0.008 mg/ml catalase and 10 mM dithiothreitol]). Then 4 µl of the kinesin solution was mixed with 96 µl of 10× diluted functionalized GeNTOPs and incubated for 10 min. About, 20 µl of this GeNTOP-motility solution was flown into the channel for single-molecule force measurements. To rule out artifacts from angled motion in the optical trap,[44] only microtubules aligned with the flow cell channel direction and perpendicular to the laser polarization[45] were chosen for experiments.

Optical tweezers setup and calibration Measurements were performed in our ultraprecision optical tweezers setup.[27,29] Briefly, the setup has near-Å resolution in surface-coupled assays (Extended Data Fig. 1) and is equipped with a millikelvin precision temperature control set to 29.500 °C.[27] Signals of a 1064 nm trapping laser were recorded with 100 kHz by back focal plane detection. The optical trap was calibrated by a combined power spectral density–drag force method.[28,29] The average trap stiffness used for experiments was about 0.05 pN/ nm. For the power spectra in Extended Data Fig. 2, the trap stiffness was 0.0552 ± 0.0005 pN/nm and 0.0561 ± 0.0005 pN/nm recorded at 2 µm and 5 µm distance from the surface using about 600 mW and 6.5 mW of laser power in the focus for the GeNTOP and polystyrene microsphere, respectively. Both trap stiffness values quantitatively agreed with Mie theory calculations for our setup[45–47] using a refractive index of 4.34 +

414 $0.016i$? for the GeNTOPs. Due to absorption, we measured a temperature increase for
415 the GeNTOPs at 600 mW trapping power of about 7 K above the flow cell temperature
416 500 nm away from the surface using our calibration method.[37] This temperature increase
417 is slightly more than what is expected for heating due to the trapping laser alone.[49] Since
418 the surface acts as a heat sink,[49] we expect that during kinesin experiments heating was
419 less. We did not notice any significant changes due to temperature, e.g. in motor speed
420 or force generation, compared to when using polystyrene microspheres with the same trap
421 stiffness.

422 **Step detection and data processing** For step detection and filtering, data was processed
423 using an optimized, automated step finding algorithm[50] based on a modified forward-and-
424 backward filter from Chung & Kennedy that we implemented in Python[33,].[50–52] The filter
425 works very efficiently in particular, for large data sets consisting of millions of data points.
426 For sufficiently large data sets, the algorithm automatically finds the optimal window
427 length for filtering and step detection according to the following idea: if we smooth the sig-
428 nal with different window lengths, the standard deviation of the smoothed signal de-
429 creases with increasing window length as long as the window length is shorter than the
430 dwell time of the steps. As soon as the window includes steps, i.e. is comparable to
431 the dwell time of the steps, the standard deviation increases again. The window length
432 with the lowest standard deviation is used as a proxy for the optimal window size that we

empirically chose to be 4/5 of the latter window length. To filter the data while preserving steps, the optimal window size is used to calculate the variance-weighted mean of the forward and backward window corresponding to the filtered data point. For our data, we used a window size of 4.8 ms. For step detection during the fast backward motion, we used the unbiased "Steppi" algorithm.[31] In selected traces (Extended Data Fig. 7), the algorithm detected steps corresponding to single exponential relaxations with a time constant consistent with the trap response time. To robustly detect sliding steps in many traces, we fixed the relaxation time constant to the expected and exemplarily verified one. To account for the different trap response times in the different directions parallel and perpendicular to the microtubule axis and assuming that the hydrodynamic drag coefficient is the same in both directions,[29] we chose a relaxation time of $\tau_\perp \kappa_\perp / \kappa_\parallel = 25\,\mu s$, where $\kappa_\parallel$ and $\kappa_\perp$ are the trap stiffness in the direction of the microtubule axis and perpendicular to it, respectively, and $\tau_\perp$ is the experimentally measured value (Fig. 3a). The average trap stiffness of $\kappa_\parallel$ and $\kappa_\perp$ was 0.051 ± 0.001 pN/nm (N = 149) and 0.041 ± 0.001 pN/nm (N = 50). To apply sideward loads during a motility event, we manually displaced the sample 50 nm in a direction perpendicular to the microtubule axis and relative to the stationary optical trap using a piezo-translation stage resulting in sideward loads of about 2 pN. For the last short step, we measured a dwell time of 58 ± 12 ms (N = 74) longer than the average τ_2 value at that force indicating that the small increase of τ_2 with force promotes the switching to

the diffusive state. Speeds as a function of force are based on linear fits to trace segments in the respective force intervals, where automatic threshold detection of force was based on the filtered data. The speed (Extended Table 1 and 2) was well described by a linear force-velocity relation with zero-load speed v_0 = 0.64 $\pm$ 0.02 µm/s and 0.22 $\pm$ 0.02 µm/s and stall force F_s = 4.92 $\pm$ 0.03 pN and 5.1 $\pm$ 0.7 pN for high and low ATP concentrations, respectively. Based on this relation and fitted parameters, the total dwell time for a hydrolysis cycle is $\tau_{\text{cycle}} = (2\delta)/(v_0(1 - F/F_s))$ (black line in top right inset Fig. 1e and inset Fig. 2), where we used δ = 4.1 nm. The force dependence of the substeps was modeled by $\tau(F) = \tau_0 \exp(Fx^{\ddagger}/(k_{\text{B}}T)) + \tau_{\text{const}}$, where for 1 mM ATP and the long dwell time τ_1 the zero-force dwell time τ_0 was 0.5 $\pm$ 0.2 ms, the distance to the transition state $x^{\ddagger}$ was 5.3 $\pm$ 0.4 nm, and the constant τ_{const} was 7 $\pm$ 2 ms (blue line in top right inset Fig. 1e). For 1 mM ATP and the short dwell time τ_2, the data was best modeled by a constant value of 6.0 $\pm$ 1.6 ms (orange line in top right inset Fig. 1e). Note that for $F < 2$ pN, a single exponential modeled the data best and we used the same value for τ_1 and τ_2. For 10 µM ATP, the zero-force dwell time τ_0 was 4 $\pm$ 2 ms and 2.1 $\pm$ 0.4 ms, the distance to the transition state $x^{\ddagger}$ was 3.8 $\pm$ 0.6 nm and 1.2 $\pm$ 0.3 nm, and the offset τ_{const} was 24 $\pm$ 6 ms and zero for τ_1 and τ_2, respectively (blue and orange line in inset Fig. 2).

Single-molecule conditions We measured the fraction of motile GeNTOPs $p_m \pm (p_m(1 - p_m)/N)^{1/2}$ (mean $\pm$ error bar) by trapping GeNTOPs incubated with different concen-

trations of kinesin motors and placing them on microtubules to await motility.[41,53] The probability that a single motor transported the GeNTOP is $p_1 = (1 - p_m)(1 - \ln(1 - p_m))$ not accounting for that a motor, bound opposite to another one, may not be able to interact simultaneously. For single-molecule experiments, the pipetted kinesin-to-GeNTOP ratio was about 20 corresponding to a motile fraction of $p_m \lesssim 30\,\%$ implying single-molecule conditions with at least 95 % confidence. To measure speed and run length of single kinesin motors on microtubules in the absence of loads, we used another custom-built optical tweezers setup combined with interference reflection microscopy (IRM).[30] Motor-coated GeNTOPs were trapped and placed on a microtubule. If the GeNTOP showed motility, the trap was turned off and IRM images were acquired at a rate of 7 frames/s (for an example, see Supplementary Video 1). Based on kymographs, the mean motor speed and run length was $0.72 \pm 0.05\,\mu$m/s and $1.1 \pm 0.4\,\mu$m (N = 12), respectively, consistent with literature values.[54–56]

Data availability The data that support the findings of this study are available from the authors on reasonable request.

38. Ma, L., Cai, Y., Li, Y., Jiao, J. & Wu, Z. Single-molecule force spectroscopy of protein-membrane interactions. *elife* **6**, 1–21 (2017).

39. Santhosh, P. B., Thomas, N., Sudhakar, S., Chadha, A. & Mani, E. Phospholipid stabilized gold nanorods: towards improved colloidal stability and biocompatibility. *Phys. Chem. Chem. Phys.* **19**, 18494–18504 (2017).

40. Brouwer, I. *et al.* Direct quantitative detection of Doc2b-induced hemifusion in optically trapped membranes. *Nat. Commun.* **6**, 1–8 (2015).

41. Bugiel, M. *et al.* Versatile microsphere attachment of GFP-labeled motors and other tagged proteins with preserved functionality. *J. Biol. Methods* **2**, 30 (2015).

42. Rothbauer, U. *et al.* A versatile nanotrap for biochemical and functional studies with fluorescent fusion proteins. *Mol. Cell Proteomics.* **7**, 282–289 (2008).

43. Bugiel, M., Böhl, E. & Schäffer, E. The kinesin-8 Kip3 switches protofilaments in a sideward random walk asymmetrically biased by force. *Biophys. J.* **108**, 2019–2027 (2015).

501 44. Bugiel, M., Jannasch, A. & Schäffer, E. Implementation and tuning of an optical
502 tweezers force-clamp feedback system. In Gennerich, A. (ed.) *Optical Tweezers:*
503 *Methods and Protocols*, chap. 5, 109–136 (Humana Press, 2016).

504 45. Mahamdeh, M., Campos, C.P & Schäffer, E. Under-filling trapping objectives opti-
505 mizes the use of the available laser power in optical tweezers. *Opt. Express* **19**, 11759
506 (2011).

507 46. Nieminen, T. A. *et al.* Optical tweezers computational toolbox. *J. Opt. A: Pure Appl.*
508 *Opt.* **9**, 196–203 (2007).

509 47. Bormuth, V. *et al.* Optical trapping of coated microspheres. *Opt. Express* **16**, 13831–
510 13844 (2008).

511 48. Jannasch, A., Mahamdeh, M. & Schäffer, E. Inertial effects of a small brownian
512 particle cause a colored power spectral density of thermal noise. *Phys. Rev. Lett.* **107**,
513 228301 (2011).

514 49. Peterman, E. J. G., Gittes, F. & Schmidt, C. F. Laser-induced heating in optical traps.
515 *Biophys. J.* **84**, 1308–1316 (2003).

516 50. Jachowski, T. J. Stepfinder: A Python package to find steps in one dimensional
517 data with low SNR. GitHub repository: `https://github.com/tobiasjj/`
518 `stepfinder` (2019).

519 51. Chung, S. H. & Kennedy, R. A. Forward-backward non-linear filtering technique for
520 extracting small biological signals from noise. *J. Neurosci. Methods* **40**, 71–86 (1991).

521 52. Smith, D. A. A quantitative method for the detection of edges in noisy time–series.
522 *Philos. Trans. R. Soc. B* **353**, 1969–1981 (1998).

523 53. Svoboda, K. & Block, S. M. Force and velocity measured for single kinesin molecules.
524 *Cell* **77**, 773–784 (1994).

525 54. Block, S., Goldstein, L. & Schnapp, B. Bead movement by single kinesin molecules
526 studied with optical tweezers. *Nature* **348**, 348–352 (1990).

527 55. Coy, D. L., Wagenbach, M. & Howard, J. Kinesin takes one 8-nm step for each ATP
528 that it hydrolyzes. *J. Biol. Chem.* **274**, 3667–3671 (1999).

529 56. Cai, D., Verhey, K. J. & Meyhöfer, E. Tracking single kinesin molecules in the cyto-
530 plasm of mammalian cells. *Biophys. J.* **92**, 4137–4144 (2007).

531 **Acknowledgements** We thank Ulrich Rothbauer (NMI, Reutlingen, Germany) for providing the
532 anti-GFP nanobody, Andreas Schnepf for the use of the Zetasizer, and Mohammed Mahamdeh, Joe
533 Howard, Martin Oettel, and Carolina Carrasco for comments on the manuscript. This work was
534 supported by the interdisciplinary "nanoBCP-Lab" funded by the Carl Zeiss Foundation (Forschungsstruk-
535 turprogramm 2017), the German Research Foundation (DFG, JA 2589/1-1, CRC1011, project

A04), the Institutional Strategy of the University of Tübingen (Deutsche Forschungsgemeinschaft, ZUK 63), and the PhD Network "Novel Nanoparticles" of the Universität Tübingen.

Author contributions S.S., and E.S. designed research; S.S. performed all experiments; S.S., M.K.A., A.J. and E.S. analysed data; M.K.A and T.J.J. provided data analysis software; T.J.J. developed the Python package stepfinder; M.B. and A.J. developed protocols, controlled statistics, and provided advice; and S.S., and E.S. wrote the paper. All authors commented on the manuscript.

Author Information The authors declare that they have no competing financial interests. Correspondence and requests for materials should be addressed to E.S. (erik.schaeffer@uni-tuebingen.de).

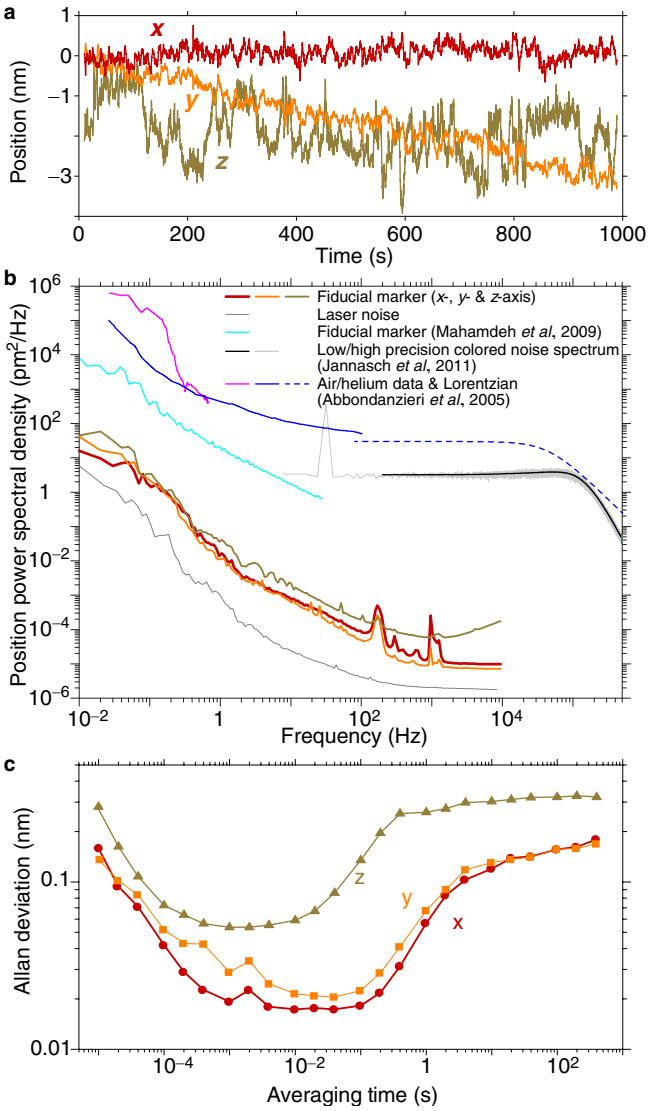

Extended Data Fig. 1 | Ultrastable optical tweezers. a, Position of a fiducial marker as a function of time (100 kHz data blocked to 10 Hz bandwidth). **b**, Position power spectral density recorded for a fiducial marker in comparison to the stability of the benchmark setup (Abbondanzieri *et al*., 2005[7]) and previously recorded data (Mahamdeh *et al*., 2009[27] and Jannasch *et al*., 2011[37]). **c**, Allan deviation as a function of lag time for the same data. Note that the setup was moved from a third-floor laboratory at the TU Dresden, Germany, where previous data[27,37] was recorded, to a basement room at the University of Tübingen, Germany, with excellent vibration and sound isolation and temperature stability.[57]

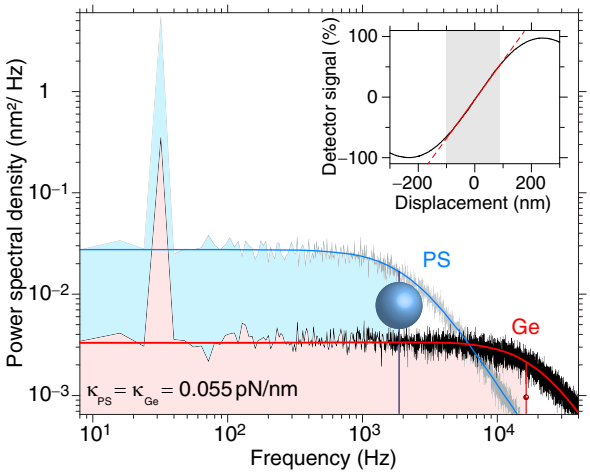

Extended Data Fig. 2 | Spatiotemporal precision of optically trapped germanium nanospheres (GeNTOPs). Power spectral density (average of 40 individual power spectra) of GeNTOP (70-nm diameter, germanium (Ge), black line) and microsphere motion (0.59-µm diameter, polystyrene (PS), grey line) trapped in water. Spectra feature a calibration peak at 32 Hz (red and blue lines, fit to theory,[28] see methods). Corner frequencies f_c are indicated by vertical lines through schematic, proportionally scaled spheres. The corner frequency serves as a measure for the available measurement bandwidth (shaded areas). Inset: lateral detector response of a surface-immobilized GeNTOP as a function of displacement relative to the trap centre (black line, linear fit red line). Because of the fluctuation-dissipation theorem, the area underneath the power spectra of the GeNTOP and microsphere motion is the same. However, power is distributed differently across the frequency space with a higher corner frequency and lower positional noise level at low frequencies for the GeNTOPs compared to the microsphere allowing for an improved spatiotemporal resolution.

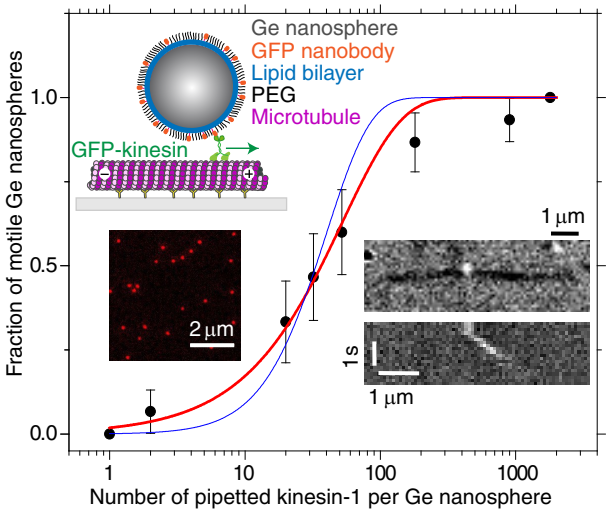

Extended Data Fig. 3 | Single kinesins transported lipid-bilayer-coated GeNTOPs. Fraction of motile GeNTOPs as a function of kinesin-to-GeNTOP ratio. Data (black circles, 40 tested nanospheres per condition) with Poisson statistics fit (transport by at least one (red line) or at least two (blue line) motors, see methods). Inset: Schematic of a kinesin motor transporting a functionalized GeNTOP along a microtubule drawn roughly to scale (top left). Confocal image of lipid bilayer-coated GeNTOPs with a membrane dye confirmed the presence of the lipid bilayer (left). Interference reflection microscopy image and kymograph (right) of a single kinesin-transported GeNTOP placed on a microtubule with the optical tweezers (bright and dark contrast, respectively).

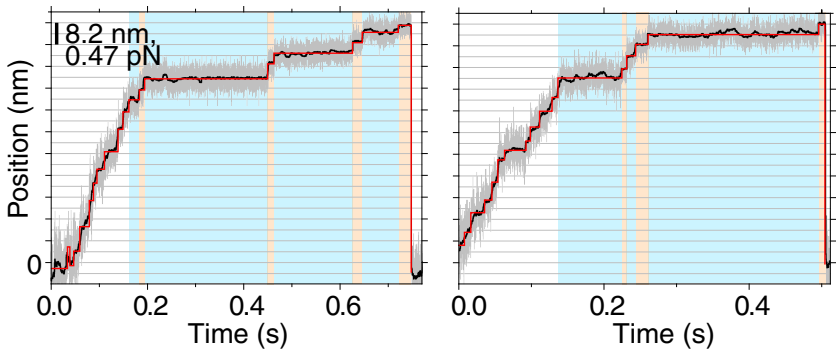

Extended Data Fig. 4 | Exemplary kinesin traces at physiological ATP concentrations. Time traces for a single-kinesin powered GeNTOP (100 kHz bandwidth, grey trace; filtered data, ≈100 Hz, black trace; detected steps, red line; see methods). Long and short dwell times τ_1 and τ_2 are blue and orange shaded, respectively.

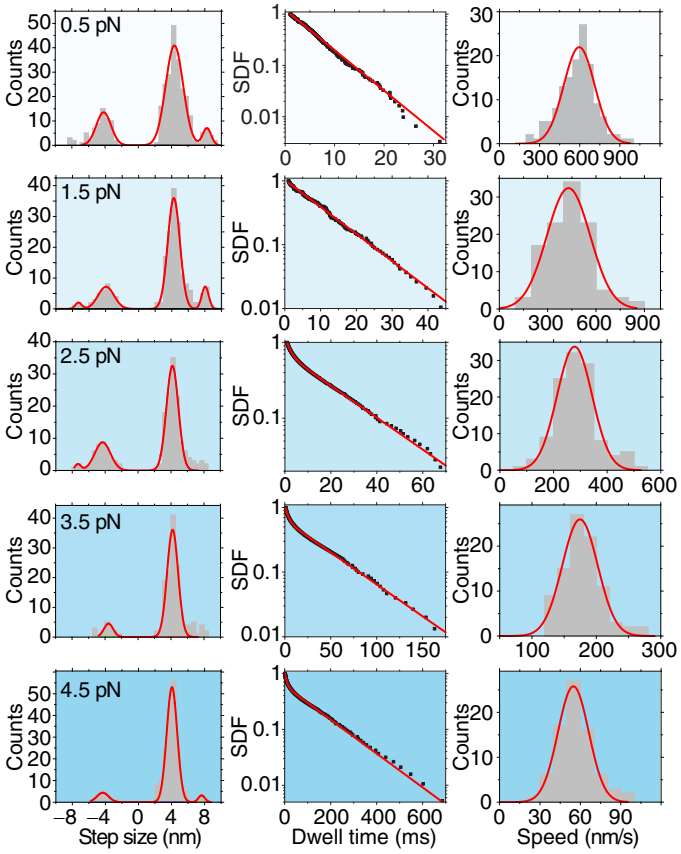

Extended Data Fig. 5 | Step size, dwell time, and speed distributions versus force at physiological ATP concentrations. Step size histograms with multi-Gaussian fit (left column), survival distribution functions (SDFs) of dwell times with fits of single or sum of two exponentials (middle column) and speed histograms with Gaussian fit (right column) for forces range with centres from 0.5 pN to 4.5 pN (top to bottom). See Extended Table 1 for fit results.

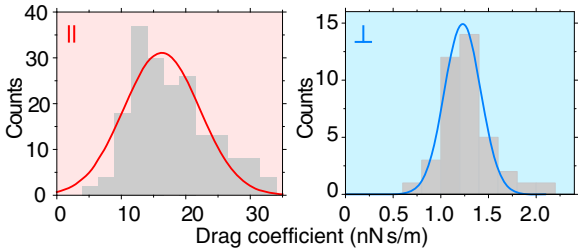

Extended Data Fig. 6 | Frictional drag coefficient based on fast backward motion. Histograms of the frictional drag coefficient measured parallel ($\gamma_{||}$, left, red shaded) and perpendicular ($\gamma_{\perp}$, right, blue shaded) to the microtubule axis with Gaussian fits (red and blue lines). The frictional drag coefficient for the two directions was calculated according to $\gamma = \tau\kappa$ using the measured values for the relaxation time and trap stiffness (see Fig. 3 and methods). The resulting values for $\gamma_{||}$ and $\gamma_{\perp}$ are 16.0 $\pm$ 0.8 nN s/m (N = 149) and 1.24 $\pm$ 0.07 nN s/m (N = 50), respectively. The latter frictional drag coefficient $\gamma_{\perp}$ was larger than the hydrodynamic (viscous) drag coefficient expected from Stokes drag and the measured GeNTOP size. The ratio between the measured coefficient $\gamma_{\perp}$ and the calculated Stokes drag coefficient is about 1.9. This increase is due to the surface proximity.[29] Based on Faxén's law, this ratio is consistent with the GeNTOP being 10 nm away from the surface.

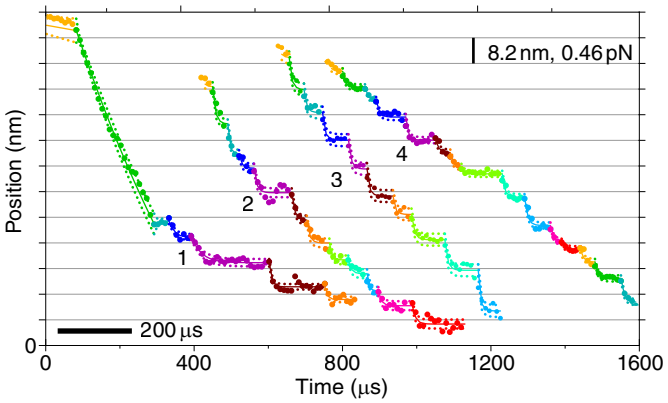

Extended Data Fig. 7 | Exemplary kinesin traces of fast, biased sliding motion in the weakly bound diffusive state. Coloured sections correspond to detected states fitted with a single exponential relaxation using the "Steppi" algorithm.[31] Traces 1 and 2 had no constraints resulting in a step size of 7.7 ± 0.1 nm and exponential relaxation time of 27 ± 3 µs (N = 20, excluding the first step of Trace 1). For Traces 3 and 4, the relaxation time constant was fixed to 25 µs (see methods). The force scale bar is based on the average trap stiffness for the four traces.

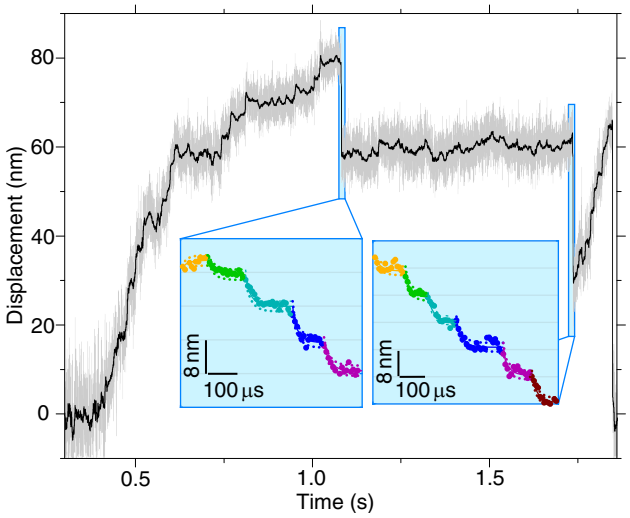

Extended Data Fig. 8 | **Exemplary kinesin trace with short slip events.** Time traces for a single-kinesin powered GeNTOP (100 kHz bandwidth, grey trace; filtered data, ≈100 Hz, black trace; see methods). Insets: Magnified view of short backward slips. Coloured sections correspond to detected states fitted with a single exponential relaxation using the "Steppi" algorithm.[31]

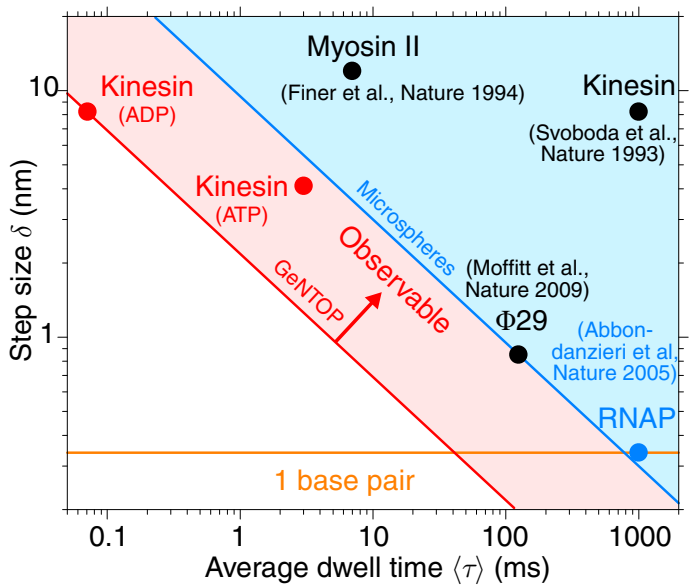

Extended Data Fig. 9 | Optical tweezers spatiotemporal resolution of molecular machines. Step size versus dwell time for various molecular machines[7,9,58,59] in comparison to this work (red circles, 4-nm directed substeps (0–1 pN data point at 10 µM ATP of Extended Table 2), fast 8-nm sliding steps (ADP state, Fig. 3a)). Blue and red line indicate previous, microsphere benchmark[7] and current GeNTOP spatiotemporal resolution (this work), respectively, according to the relation $\delta\sqrt{\langle\tau\rangle}$.[2] The half space above the lines is observable.

Extended Data Table 1 | Step size, dwell time and speed versus force at 1 mM ATP.

F	δ_+ (nm)	p	δ_- (nm)	p	τ_1 (ms)	p	τ_2 (ms)	p	v (µm/s)
0–1	4.34 ± 0.06 (217)	72	4.2 ± 0.2 (65)	22	5.5 ± 0.2 (306)	120	–	–	0.60 ± 0.01 (134)
	8.2 ± 0.6 (19)	6							
1–2	4.25 ± 0.04 (140)	72	4.0 ± 0.2 (34)	18	10.3 ± 0.8 (193)	103	–	–	0.43 ± 0.01 (110)
	7.8 ± 0.2 (15)	8	8.2 ± 0.6 (4)	2					
2–3	4.19 ± 0.04 (127)	71	4.1 ± 0.2 (42)	25	20.6 ± 0.1 (100)	71	2.1 ± 0.7 (78)	50	0.28 ± 0.01 (117)
	7.3 ± 0.5 (4)	2	7.3 ± 0.5 (5)	2					
3–4	4.18 ± 0.05 (127)	85	3.9 ± 0.4 (16)	10	44.7 ± 0.4 (84)	63	3.3 ± 0.7 (66)	49	0.18 ± 0.01 (112)
	7.8 ± 0.2 (7)	5							
$\geq$4	4.06 ± 0.03 (168)	89	4.3 ± 0.4 (16)	8	144 ± 2 (104)	60	8.8 ± 0.2 (86)	47	0.055 ± 0.001 (92)
	7.6 ± 0.4 (6)	3							

F (pN): force, $\delta_{+/-}$: forward/backward step size (Gaussian centre $\pm$ fit error (N based on area underneath Gaussian normalized by total number of steps)), p (%): relative percentage, τ: dwell time based on survival function fit (N according to relative amount), and v: speed (mean $\pm$ standard error (N: number of trace segments fitted)). All fits to data of Extended Data Fig. 5. Note that only few data points correspond to forces larger than 5 pN. Also note that p-values for dwell times directly reflect the fitted amplitude that may add up to more than 100 % indicating that some of the expected very short steps were missed. Errors on all percentages are less than 1 %.

Extended Data Table 2 | Step size, dwell time and speed versus force at 10 µM ATP.

F	δ_+ (nm)	p	δ_- (nm)	p	τ_1 (ms)	p	τ_2 (ms)	p	υ (µm/s)
0–1	4.13 ± 0.06 (53)	67	4.2 ± 0.2 (15)	20	30.2 ± 0.6 (44)	65	3.1 ± 0.2 (34)	47	0.23 ± 0.01 (12)
	7.2 ± 0.2 (10)	13							
1–2	4.15 ± 0.03 (53)	69	4.5 ± 0.4 (9)	11	37.8 ± 0.7 (42)	61	3.3 ± 0.1 (34)	49	0.16 ± 0.01 (17)
	7.6 ± 0.36 (15)	20							
2–3	4.05 ± 0.03 (59)	78	4.5 ± 0.5 (7)	9	54.3 ± 0.1 (40)	58	3.8 ± 0.1 (37)	52	0.110 ± 0.007 (13)
	7.5 ± 0.17 (10)	13							
3–4	4.17 ± 0.05 (42)	70	4.3 ± 0.2 (6)	10	131 ± 3 (33)	57	6.8 ± 0.3 (27)	45	0.056 ± 0.005 (15)
	7.84 ± 0.36 (12)	20							
$\geq$4	4.12 ± 0.04 (77)	85	3.9 ± 0.2 (6)	7	245 ± 5 (41)	56	8.0 ± 0.3 (40)	45	0.032 ± 0.004 (15)
	8.12 ± 0.13 (7)	8							

F (pN): force, $\delta_{+/-}$: forward/backward step size (Gaussian centre $\pm$ fit error (N based on area underneath Gaussian normalized by total number of steps)), p (%): relative percentage, τ: dwell time based on survival function fit (N according to relative amount), and υ: speed (mean $\pm$ standard error (N: number of trace segments fitted)). Note that only few data points correspond to forces larger than 5 pN. Also note that p-values for dwell times directly reflect the fitted amplitude that may add up to more than 100 % indicating that some of the expected very short steps were missed. Errors on all percentages are less than 1 %.

Extended Data References

57. Hermsdorf, G. L., Szilagyi, S. A., Rösch, S. & Schäffer, E. High performance passive vibration isolation system for optical tables using six-degree-of-freedom viscous damping combined with steel springs. *Rev. Sci. Instrum.* **90**, 015113 (2019).

58. Finer, J. T., Simmons, R. M. & Spudich, J. A. Single myosin molecule mechanics : piconewton forces and nanometre steps. *Nature* **368**, 113–119 (1994).

59. Moffitt, J. R. *et al.* Intersubunit coordination in a homomeric ring ATPase. *Nature* **457**, 446–450 (2009).